Persistent exchange splitting in the chiral helimagnet $Cr_{1/3}NbS_2$

Na Qin,[1,*] Cheng Chen,[2,*] Shiqiao Du,[1,*] Xian Du,[1] Xin Zhang,[3] Zhongxu Yin,[1] Jingsong Zhou,[1] Runzhe Xu,[1] Xu Gu,[1] Qinqin Zhang,[1] Wenxuan Zhao,[1] Yidian Li,[1] Sung-Kwan Mo,[2] Zhongkai Liu,[3,4] Shilei Zhang,[3,4] Yanfeng Guo,[3,4] Peizhe Tang,[5,6] Yulin Chen,[1,3,4,7,†] and Lexian Yang[1,8,‡]

[1]*State Key Laboratory of Low Dimensional Quantum Physics, Department of Physics, Tsinghua University, Beijing 100084, China*

[2]*Advanced Light Source, Lawrence Berkeley National Laboratory, Berkeley, California 94720, USA*

[3]*School of Physical Science and Technology, ShanghaiTech University and CAS-Shanghai Science Research Center, Shanghai 201210, China*

[4]*ShanghaiTech Laboratory for Topological Physics, Shanghai 200031, China*

[5]*School of Materials Science and Engineering, Beihang University, Beijing 100191, China*

[6]*Max Planck Institute for the Structure and Dynamics of Matter, Center for Free Electron Laser Science, 22761 Hamburg, Germany*

[7]*Department of Physics, Clarendon Laboratory, University of Oxford, Parks Road, Oxford OX1 3PU, UK*

[8]*Frontier Science Center for Quantum Information, Beijing 100084, China*

(Received 23 February 2022; revised 4 May 2022; accepted 29 June 2022; published 18 July 2022)

Using high-resolution angle-resolved photoemission spectroscopy and *ab initio* calculation, we systematically investigate the electronic structure of the chiral helimagnet $Cr_{1/3}NbS_2$ and its temperature evolution. The comparison with NbS_2 suggests that the electronic structure of $Cr_{1/3}NbS_2$ is strongly modified by the intercalation of Cr atoms. Our *ab initio* calculation, consistent with experimental results, suggests strong hybridization between Nb- and Cr-derived states near the Fermi level. In the chiral helimagnetic state (below the Curie temperature, T_c), we observe exchange splitting of the energy bands crossing the Fermi level, which follows the temperature evolution of the magnetic moment, suggesting a strong interaction between the conduction electrons and Cr spin moments. Interestingly, the exchange splitting persists far above T_c with weak temperature dependence, in drastic contrast to the itinerant ferromagnetism described by the Stoner model, indicating the existence of short-range magnetic order. Our results provide important insights into the interplay between the electronic structure and magnetism in $Cr_{1/3}NbS_2$, which is helpful for understanding the microscopic mechanism of chiral helimagnetic ordering.

DOI: 10.1103/PhysRevB.106.035129

I. INTRODUCTION

Chiral materials lacking both inversion and mirror symmetries exhibit many interesting properties, such as chiral Weyl fermions and extremely long Fermi arcs [1–6], a quantized circular photogalvanic current [7], and a chiral magnetic effect [8]. Particularly, if a chiral material hosts magnetic ordering, the competition between the ferromagnetic (FM) exchange interaction and the Dzyaloshinskii–Moriya interaction (DMI) can result in helical alignment of spins, forming the so-called chiral helimagnet (CHM). CHMs can harbor novel topological excitation with magnetic vortices known as skyrmions that can be effectively tuned by external magnetic field or spin-polarized electrical currents [9–12], promising great application potential for spintronic devices. So far, CHM materials have been discovered in mainly two space groups: cubic space group $P2_13$, such as MnSi [9,13], $Fe_{1-x}Co_xSi$ [14,15], FeGe [16–18], Cu_2OSeO_3 [19,20]; and cubic space group $P4_132$ or $P4_332$, such as β-Mn-type Co-Zn-Mn [21] and $FePtMo_3N$ [22].

Among the CHMs, $Cr_{1/3}NbS_2$ is unique since it hosts a one-dimensional chiral soliton lattice instead of two-dimensional or three-dimensional skyrmions [23]. It crystallizes in a layered hexagonal structure with the space group of $P6_322$. Within each unit cell, there are two trigonal prismatic NbS_2 layers that are rotated by 180° with respect to each other. The Cr atoms occupy the octahedral holes between two adjacent NbS_2 layers and order in a $(\sqrt{3}\times\sqrt{3})R(30^\circ)$ superstructure. $Cr_{1/3}NbS_2$ can therefore be considered as Cr-intercalated 2H-NbS_2 [Fig. 1(a)]. Below about 125 K, the intercalated Cr atoms with a local spin moment of about 3 μ_B order ferromagnetically and the system enters into a helimagnetic ground state with a large helix period of 48 nm along the chiral c-axis [Fig. 1(b)]. The difference in the magnetic moment measured under field cooling (FC) and zero field cooling (ZFC) conditions in Fig. 1(c) suggests a ferromagnetic transition in $Cr_{1/3}NbS_2$. When an external magnetic field is applied perpendicular to the c-axis, a highly tunable and robust chiral soliton lattice can be observed [23], indicating the important application potential in spintronic devices.

Despite extensive research effort, the microscopic mechanism of the CHM ordering in $Cr_{1/3}NbS_2$ is still controversial. According to conventional understanding of magnetically intercalated transition metal dichalcogenides, the FM exchange interaction between Cr ions has a Ruderman–Kittel–Kasuya–Yosida (RKKY) form that is mediated by the itinerant Nb conduction electrons [24,25]. In this scenario, the local

*These authors contributed equally to this work.
†yulin.chen@physics.ox.ac.uk
‡lxyang@tsinghua.edu.cn

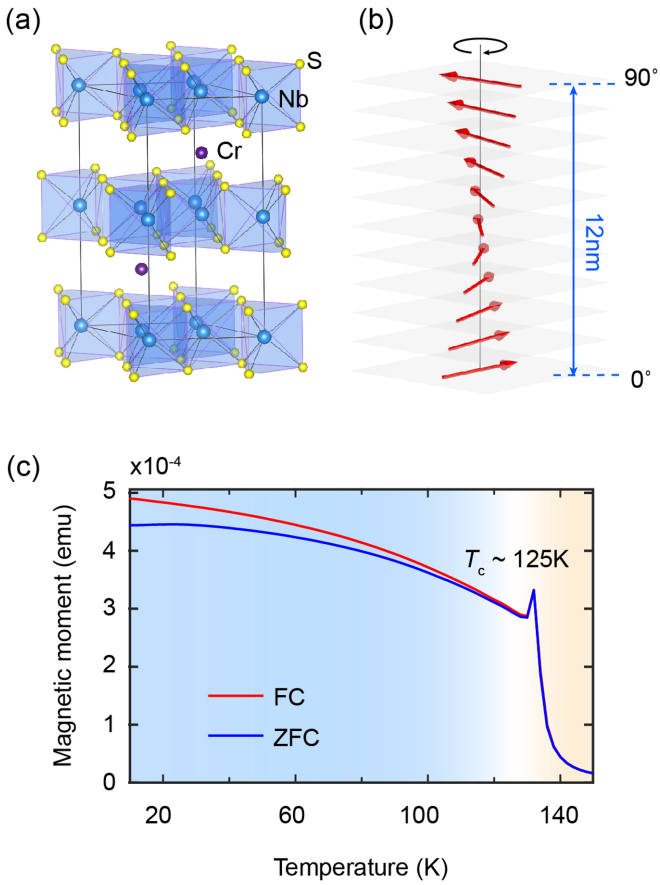

FIG. 1. (a) Crystal structure of $Cr_{1/3}NbS_2$. Cr atoms are intercalated in 2H-NbS_2, occupying the octahedral interstitial sites between two NbS_2 layers and forming a $(\sqrt{3} \times \sqrt{3})R(30^\circ)$ superstructure. (b) Schematic illustration of the magnetic helix along the *c*-axis showing 1/4 period. (c) Magnetic moment as a function of temperature measured by heating the sample under a magnetic field of 100 Oe parallel to the *ab* plane. The sample was cooled down to 15 K under a magnetic field of 1 T and without magnetic field for the FC and ZFC measurements, respectively.

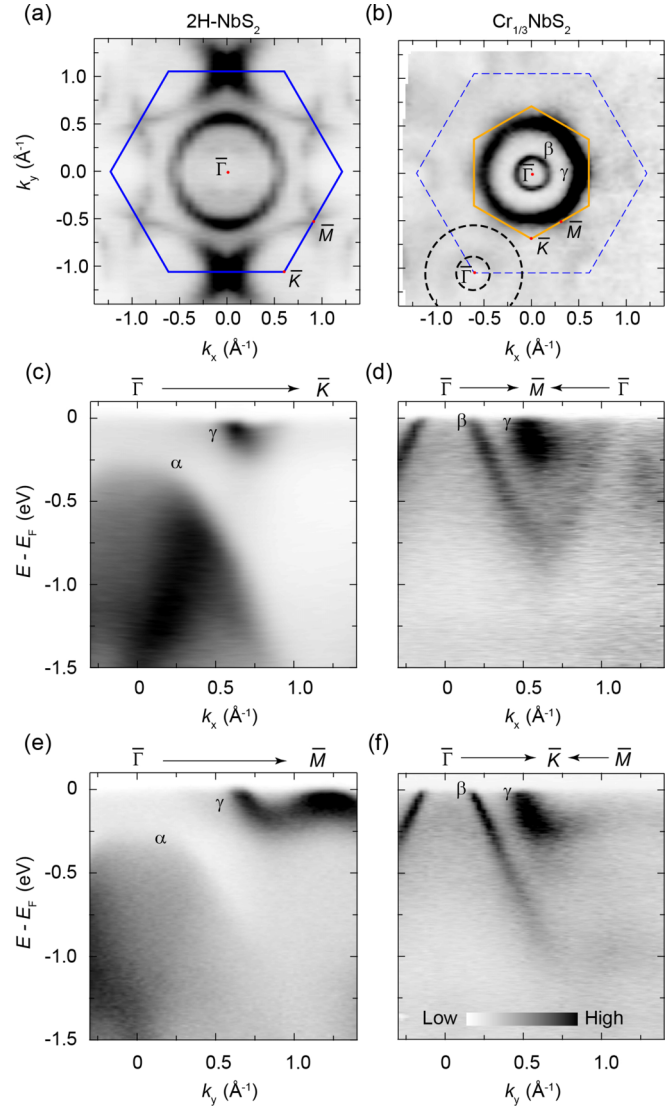

FIG. 2. (a), (b) Fermi surface of NbS_2 (a) and $Cr_{1/3}NbS_2$ (b) measured by integrating ARPES intensity over an energy window of 30 meV near the Fermi level (E_F). (c)–(f) Band structure of NbS_2 (c, e) and $Cr_{1/3}NbS_2$ (d, f) along high-symmetry directions as indicated. Data of NbS_2 ($Cr_{1/3}NbS_2$) were collected using 90-eV photons at 12 (20) K.

orbitals of Cr ions contribute negligibly to the Fermi surface (FS) of $Cr_{1/3}NbS_2$, but only dope electrons to the system. However, this picture has been challenged by recent experimental [26] and theoretical [24,26,27] results, which suggest a significant contribution of Cr ions to the density of states near the Fermi level (E_F). Indeed, previous angle-resolved photoemission spectroscopy (ARPES) experiments show strong hybridization between Nb- and Cr-derived electronic states near E_F [28,29], and a Hund's exchange interaction—instead of the RKKY interaction—between Cr ions has been proposed [29]. To understand the mechanism of the novel magnetic ordering, it is essential to study adequately the electronic structure and its interplay with the magnetism of $Cr_{1/3}NbS_2$.

In this work, we systematically study the electronic structure of $Cr_{1/3}NbS_2$ and its temperature evolution using high-resolution ARPES. We reveal a drastic difference between the electronic structures of NbS_2 and $Cr_{1/3}NbS_2$, consistent with our *ab initio* calculation that suggests strong hybridization between Cr- and Nb-derived states near E_F. In the CHM state, we observe exchange splitting of energy bands crossing E_F, with a magnitude that nicely follows the temperature evolution of the magnetic moment below the Curie temperature T_c, indicating strong coupling between itinerant conduction electrons and Cr spin moments. Interestingly, the exchange splitting persists even at temperatures far above T_c, in drastic contrast to the itinerant FM described by the Stoner model. Our results suggest an important role of short-range magnetic interaction in $Cr_{1/3}NbS_2$, which will help understand the interplay between the electronic structure and magnetism in the system.

II. METHODS

The $Cr_{1/3}NbS_2$ crystals were grown via employing the chemical vapor transport method by using iodine as the

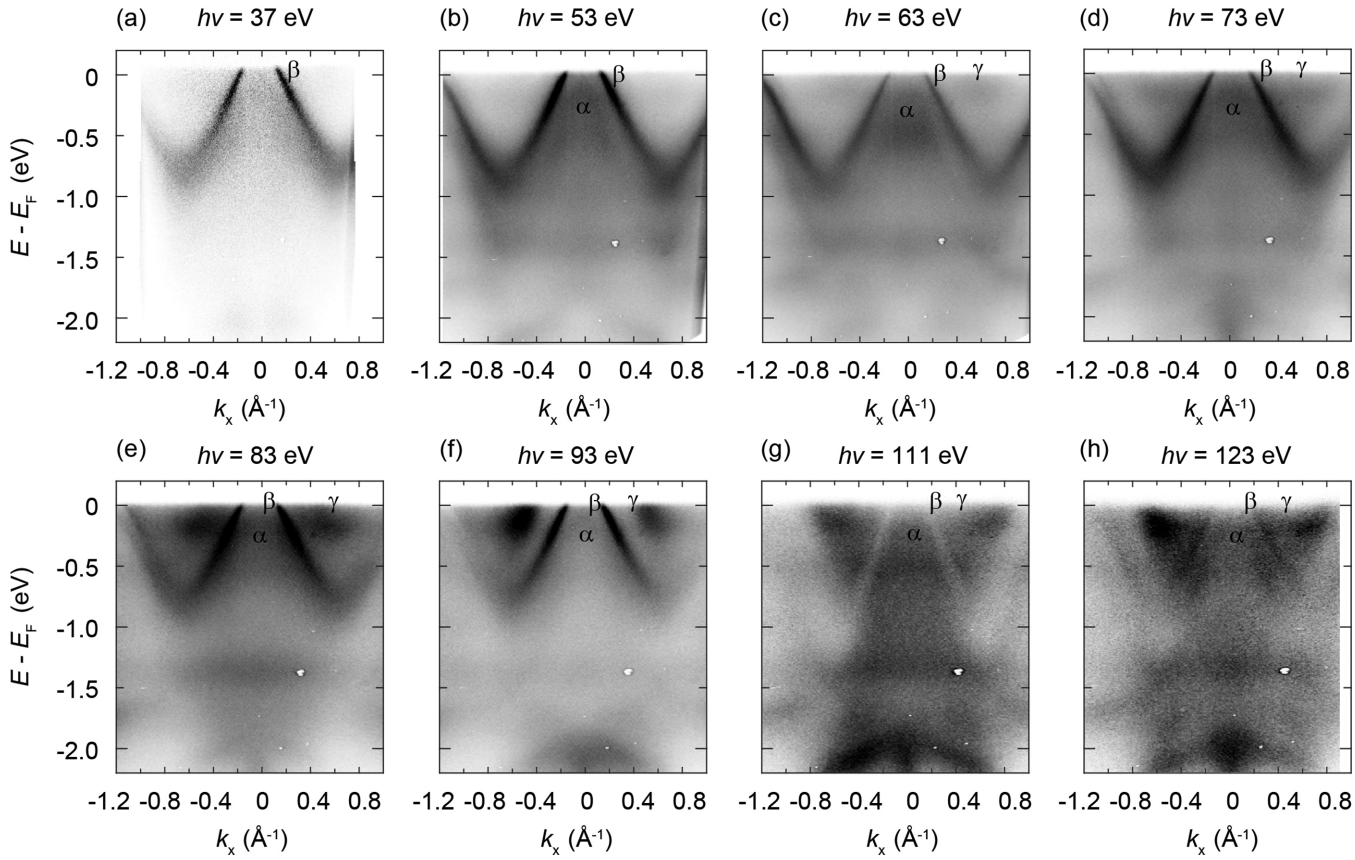

FIG. 3. (a)–(h) Band structure of $Cr_{1/3}NbS_2$ along $\bar{\Gamma}\bar{M}$ measured at selected photon energies. Data were measured at 20 K.

transfer agent. Stoichiometric Cr powder (99.9%, Adamas), Nb powder (99.95%, Aladdin), and S powder (99.9%, Adamas) were mixed and ground in a mortar. Then the mixture was sealed in a quartz tube together with the iodine in a vacuum of 10^{-4} Pa. The assembly was placed into a single temperature-zone tube furnace and the temperature of the high-temperature region was kept at 1000 °C. After two weeks, large crystals of $Cr_{1/3}NbS_2$ were obtained at the cold end of the quartz tube. The crystallographic phase and crystal quality examinations of $Cr_{1/3}NbS_2$ were performed on a single-crystal x-ray diffractometer equipped with a Mo Kα radioactive source ($\lambda = 0.71073$ Å). The diffraction patterns could be satisfyingly indexed on the basis of a Nb_3CoS_6 polytype structure (space group: $P6_322$, No. 182) with the lattice parameters $a = b = 5.74$ Å, $c = 12.09$ Å, $\alpha = 90°$, $\beta = 90°$, and $\gamma = 120°$.

High-resolution ARPES measurements were performed at beamline 13U of National Synchrotron Radiation Laboratory (NSRL), beamlines 4.0.3 and 10.0.1 of Advanced Light Source (ALS), and beamline 5-4 of Stanford Synchrotron Radiation Light Source (SSRL). Data were collected with a Scienta R4000 (DA30) electron analyzer at NSRL and ALS (SSRL). The overall energy and angular resolutions were set to 15 meV and 0.2°, respectively. The samples were cleaved *in situ* and measured under ultra-high vacuum less than 1.0×10^{-10} mbar.

First-principles band structure calculations were performed using the QUANTUM ESPRESSO code package [30] for the nonmagnetic calculations and the Vienna *ab initio* simulation package (VASP) [31] for the magnetic calculations with plane-wave basis. The exchange–correlation energy was considered under a Perdew–Burke–Ernzerhof-type generalized gradient approximation (GGA) [32]. For the calculation of $Cr_{1/3}NbS_2$, the GGA + U method was applied to describe the 3*d*-orbitals of Cr atoms, where on-site Coulomb interaction U was set to 4 eV. Spin-orbit coupling was not included due to its minor effect on band structure. Experimental lattice parameters were used. The cutoff energy for the plane-wave basis was set to 480 eV for calculations with QUANTUM ESPRESSO and 400 eV for calculations with VASP. A Γ-centered Monkhorst–Pack k-point mesh of $9 \times 9 \times 4$ with a spacing of 0.15 Å^{-1} was adopted in all self-consistent calculations.

III. RESULTS AND DISCUSSIONS

Figure 2 shows the comparative study of the electronic structure of NbS_2 and $Cr_{1/3}NbS_2$. On the FS of NbS_2, we observe a large hole pocket around the $\bar{\Gamma}$ and $\bar{K}$ points, respectively [Fig. 2(a)]. We do not observe the band splitting caused by the coupling between the two NbS_2 layers in one unit cell [33]. In $Cr_{1/3}NbS_2$, by contrast, we observe an extra small hole pocket around the $\bar{\Gamma}$ point [Fig. 2(b)]. Due to the $(\sqrt{3} \times \sqrt{3})R(30°)$ superstructure, the Brillouin zone (BZ) of $Cr_{1/3}NbS_2$ is rotated by 30° and shrinks by 2/3, compared to the BZ of NbS_2. Along $\bar{\Gamma}\bar{K}$ and $\bar{\Gamma}\bar{M}$, we observe only one band crossing E_F in NbS_2, while there are two bands, marked as β and γ, crossing E_F along $\bar{\Gamma}\bar{K}\bar{M}$ and $\bar{\Gamma}\bar{M}\bar{\Gamma}$ in $Cr_{1/3}NbS_2$

[Fig. 2(c)–2(f)]. The β band shows up only in $Cr_{1/3}NbS_2$, suggesting that the Cr-derived electron states contribute significantly to the electronic structure near E_F.

Figure 3(a)–3(h) shows the band structure of $Cr_{1/3}NbS_2$ measured with different photon energies, which can measure the k_z dispersion of energy bands and reflects the interlayer coupling. Both the β and γ bands show weak k_z dependence, except that the spectral weight of the γ band is enhanced at high photon energies due to the matrix element effect. We observe an extra α band with its band top touching E_F. It shows a continuum-like spectral weight distribution, suggesting its strong k_z dispersion, similar to the α band in NbS_2 [Fig. 2(c)]. Apparently, the electronic structure of $Cr_{1/3}NbS_2$ cannot be derived from a rigid shift of the electronic structure of NbS_2 induced by electron donation from Cr ions. Although the overall dispersion of the α and γ bands are very similar in NbS_2 and $Cr_{1/3}NbS_2$, their relative energy positions are different. The α band shifts toward E_F for about 250 meV, while the γ band shifts toward higher binding energies for about 100 meV in $Cr_{1/3}NbS_2$. Therefore, the electronic structure of $Cr_{1/3}NbS_2$ cannot be derived from electron doping in NbS_2 by Cr intercalation. Moreover, the k_z dispersion of the α band also suggests an important role of interlayer coupling in the electronic structure and magnetic properties of $Cr_{1/3}NbS_2$.

To understand further the influence of Cr atoms on the electronic structure of $Cr_{1/3}NbS_2$, we perform an *ab initio* calculation on the electronic structures of NbS_2 and $Cr_{1/3}NbS_2$, as illustrated in Fig. 4. For better comparison, the result of NbS_2 is artificially folded into a $(\sqrt{3}\times\sqrt{3})R(30^\circ)$ superstructured BZ similar to that of $Cr_{1/3}NbS_2$. Figure 4(a) and 4(b) compares the electronic structures of NbS_2 and paramagnetic $Cr_{1/3}NbS_2$ (onsite Coulomb interaction $U = 4\,eV$). Apparently, the electronic structure of $Cr_{1/3}NbS_2$ cannot be understood by electron doping from intercalated Cr ions. Rather, the number of energy bands crossing E_F increases due to the hybridization between the Cr- and Nb-derived states, consistent with our experiment in Fig. 2. In the FM state, we observe spin-splitting of the energy bands due to the exchange interaction [Fig. 4(c)]. In Fig. 4(d), we compare the calculated electronic structure of $Cr_{1/3}NbS_2$ in the CHM and FM states. No noticeable difference is observed, suggesting the same influence of the CHM and FM ordering on the electronic structure, which is reasonable considering the large helix period of the CHM state [24,26,27]. Therefore, the DMI that is responsible for the spiral spin ordering serves as a weak perturbation to the FM state [26]. Figure 4(e) shows the orbital-projected calculation of the electronic structure of $Cr_{1/3}NbS_2$ in the FM state. We observe a substantial spectral weight of Cr d-orbitals near E_F, confirming the strong hybridization between the Cr- and Nb-derived states, consistent with previous *ab initio* calculations [24,26,27].

Both our experiments and calculations are in good agreement with previous results. Nevertheless, it is noteworthy that due to the electronic correlation of Cr d-states, the multiband nature of the system, and complicated magnetic ordering, there still exist clear deviations between the ARPES measured and calculated electronic structure of $Cr_{1/3}NbS_2$ [24,26–29]. For example, in the FM state, there are more bands crossing E_F in the calculation, and some calculated bands are missing in the experiments (Supplemental Materials Fig. S2

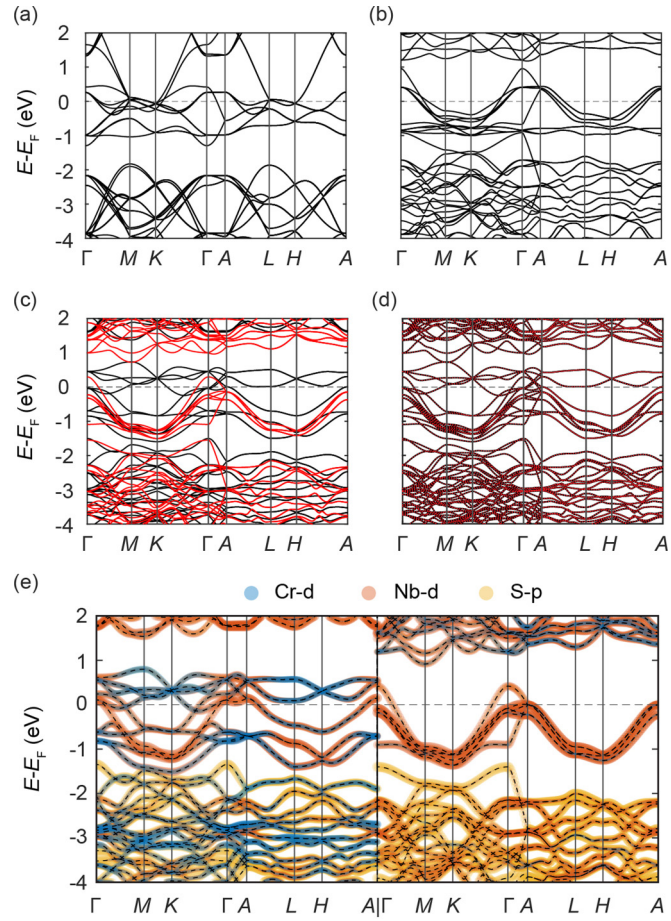

FIG. 4. (a)–(e) *Ab initio* calculation of the electronic structure of NbS_2 (a) and $Cr_{1/3}NbS_2$ (b–e). The calculation in (a) is folded into a $(\sqrt{3}\times\sqrt{3})R(30^\circ)$ superstructured BZ for better comparison with the result in $Cr_{1/3}NbS_2$. The calculations in (b) and (c) were performed for paramagnetic and FM states, respectively. The black (red) lines in (c) represent spin up (down) bands. (d) Comparison between the calculated electronic structure in the CHM (solid black) and FM (dotted red) states showing a negligible difference. (e) Orbital-projected calculation of the spin-split band structure of the FM state (left: spin up, right: spin down).

[34]). Further experimental and theoretical investigations are highly demanded to understand fully the electronic structure of $Cr_{1/3}NbS_2$.

Figure 5 tracks the temperature evolution of the band structure of $Cr_{1/3}NbS_2$ measured with improved energy resolution using relatively low photon energy. Figure 5(a)–5(e) show ARPES intensity maps at selected temperatures. In the CHM state at 15 K, we observe four bands near E_F, marked as α, β_1, β_2, and γ in Fig. 5(a), compared to the two bands β and γ in Fig. 2. With increasing temperature, the splitting between β_1 and β_2 gradually decreases and can hardly be resolved at 195 K. To quantify the evolution of the band structure, we collect the momentum distribution curves (MDCs) at E_F taken at different temperatures [Fig. 5(f)] and fit each MDC to multiple Lorentzians. The extracted Fermi crossings of the β_1, β_2, and γ bands are overlaid on the false-color plot of the MDCs in Fig. 5(g). The β_1 and β_2 bands approach each other with increased temperature, with a sudden change of their splitting

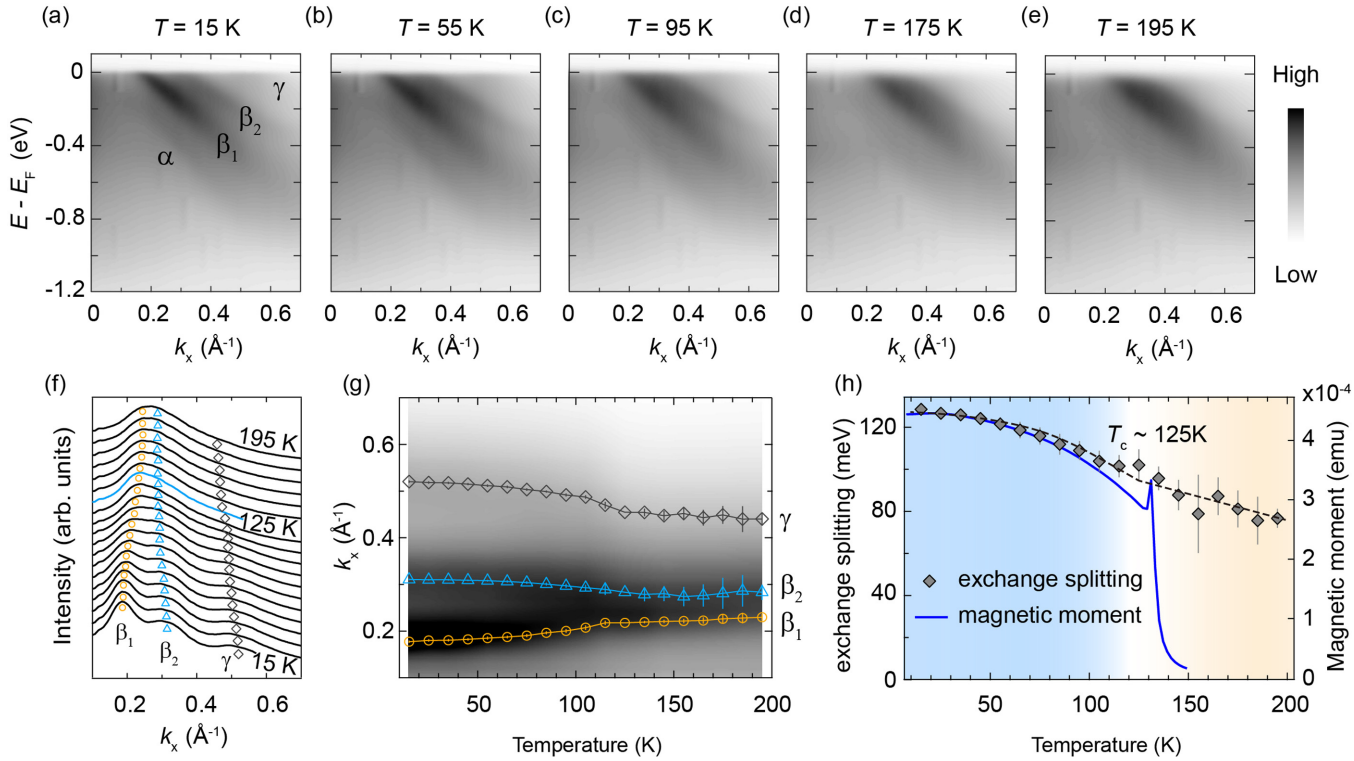

FIG. 5. (a)–(e) Band structure of $Cr_{1/3}NbS_2$ along $\bar{\Gamma}\bar{M}$ measured at selected temperatures. (f) Temperature evolution of the MDCs at E_F. The colored markers are a guide to help one note the temperature evolution of the peak positions. (g) False-color plot of the temperature evolution of the MDCs at E_F. The orange circles, blue triangles, and gray diamonds indicate MDC peak positions extracted by fitting the MDCs to multiple Lorentzians. (h) The exchange splitting between the β_1 and β_2 bands as a function of temperature (Supplementary Materials Fig. S1 [34]). The dashed line is a guide to help one note the evolution of the exchange splitting. The temperature evolution of the magnetic moment is also shown for comparison.

near 125 K, where the γ band also shows a sudden change of its position. From the temperature evolution of the energy bands, we conclude that the FM ordering strongly influences the band structure of $Cr_{1/3}NbS_2$, and the splitting between the β_1 and β_2 bands is the exchange splitting caused by the FM ordering.

In general, as described by the Stoner model, if the long-range FM order is mainly contributed by the itinerant electron around E_F, the magnitude of exchange splitting in metallic FM materials is proportional to the magnetic moment and becomes zero above T_c. In Fig. 5(h), we compare the temperature evolution of the exchange splitting and the magnetic moment. Below T_c, the exchange splitting follows the increasing magnetic moment with decreasing temperature, suggesting a strong interplay between the conduction carriers and the magnetic moment of the system. Above T_c, interestingly, the exchange splitting deviates from the magnetic moment curve and persists up to at least 195 K [Fig. 5(g) and 5(h)], in drastic contrast to the Stoner model, suggesting that $Cr_{1/3}NbS_2$ is not a band magnetic material.

The exchange splitting that is persistent above T_c has been widely observed in metallic ferromagnets, including Fe, Ni, $SrRuO_3$, and Fe_3GeTe_2 [35–40], despite the controversial experimental results in Ni [41]. However, the temperature dependence of the exchange splitting is quite different in these materials. In $SrRuO_3$ and Fe_3GeTe_2, the bands stay put with increasing temperature, suggesting a minor impact of long-range magnetic ordering on the exchange splitting [38,39], consistent with a localized intra-atomic exchange interaction [35]. By contrast, the exchange splitting in $Cr_{1/3}NbS_2$ strictly follows the magnetic moment below T_c, but shows minor temperature dependence above T_c. We emphasize that, despite the helimagnetic nature of $Cr_{1/3}NbS_2$, the exchange spitting is mainly induced by the FM order in the system [Fig. 4(d)] [26]. Therefore, similar to the previous result in Ni [35], the observed temperature evolution of the exchange spitting may be understood within the Oguchi model that describes short-range order by exactly treating the interactions between neighboring magnetic ion pairs while approximating the other pairs with a mean field [35]. Consistently, previous measurements of critical exponents support the short-range magnetic coupling between Cr atoms [42,43]. On the other hand, the persistent exchange splitting above T_c can also be induced by the formation of short-range FM order, such as the Griffith phase, in which finite-size FM clusters exist in the paramagnetic phase at high temperatures [44]. Further detailed experimental and theoretical works are required to understand fully the observed exchange spitting at temperatures far above T_c.

IV. CONCLUSION

In conclusion, we have systematically investigated the electronic structure of the CHM $Cr_{1/3}NbS_2$ and its temperature evolution. Both experimental results and *ab initio* calculations show strong hybridization between the Cr- and Nb-derived states near E_F, in contrast to a simple Cr-doping rigid-shift scenario. Moreover, we observed exchange splitting of the band structure that persists far above T_c, which is beyond expectation of a band magnetism and suggests the existence of short-range magnetic order in $Cr_{1/3}NbS_2$. Our results provide important insight into the understanding of the electronic and magnetic properties of the monoaxis CHM $Cr_{1/3}NbS_2$.

ACKNOWLEDGMENTS

This work was supported by the National Natural Science Foundation of China (Grants No. 11774190, No. 11427903, No. 11634009), the National Key R&D Program of China (Grants No. 2017YFA0304600, No. 2017YFA0305400, and No. 2017YFA0402900), and EPSRC Platform Grant (Grant No. EP/M020517/1). Use of the Stanford Synchrotron Radiation Light Source, SLAC National Accelerator Laboratory, is supported by the US Department of Energy, Office of Science, Office of Basic Energy Sciences under Contract No. DE-AC02-76SF00515. This research used resources of the Advanced Light Source, a US Department of Energy Office of Science User Facility under Contract No. DE-AC02-05CH11231.

[1] N. B. M. Schröter, D. Pei, M. G. Vergniory, Y. Sun, K. Manna, F. de Juan, J. A. Krieger, V. Süss, M. Schmidt, P. Dudin, B. Bradlyn, T. K. Kim, T. Schmitt, C. Cacho, C. Felser, V. N. Strocov, and Y. Chen, Nat. Phys. **15**, 759 (2019).

[2] N. B. M. Schröter, S. Stolz, K. Manna, F. de Juan, M. G. Vergniory, J. A. Krieger, D. Pei, T. Schmitt, P. Dudin, T. K. Kim, C. Cacho, B. Bradlyn, H. Borrmann, M. Schmidt, R. Widmer, V. N. Strocov, and C. Felser, Science **369**, 179 (2020).

[3] Z. Rao *et al.*, Nature **567**, 496 (2019).

[4] D. Takane, Z. Wang, S. Souma, K. Nakayama, T. Nakamura, H. Oinuma, Y. Nakata, H. Iwasawa, C. Cacho, T. Kim, K. Horiba, H. Kumigashira, T. Takahashi, Y. Ando, and T. Sato, Phys. Rev. Lett. **122**, 076402 (2019).

[5] D. S. Sanchez *et al.*, Nature (London) **567**, 500 (2019).

[6] B. Q. Lv, Z. L. Feng, J. Z. Zhao, N. F. Q. Yuan, A. Zong, K. F. Luo, R. Yu, Y. B. Huang, V. N. Strocov, A. Chikina, A. A. Soluyanov, N. Gedik, Y. G. Shi, T. Qian, and H. Ding, Phys. Rev. B **99**, 241104(R) (2019).

[7] Z. Ni, K. Wang, Y. Zhang, O. Pozo, B. Xu, X. Han, K. Manna, J. Paglione, C. Felser, A. G. Grushin, F. de Juan, E. J. Mele, and L. Wu, Nat. Commun. **12**, 154 (2021).

[8] G. Chang, B. J. Wieder, F. Schindler, D. S. Sanchez, I. Belopolski, S.-M. Huang, B. Singh, D. Wu, T.-R. Chang, T. Neupert, S.-Y. Xu, H. Lin, and M. Z. Hasan, Nat. Mater. **17**, 978 (2018).

[9] S. Mühlbauer, B. Binz, F. Jonietz, C. Pfleiderer, A. Rosch, A. Neubauer, R. Georgii, and P. Böni, Science **323**, 915 (2009).

[10] U. K. Rößler, A. N. Bogdanov, and C. Pfleiderer, Nature (London) **442**, 797 (2006).

[11] N. Romming, C. Hanneken, M. Menzel, J. E. Bickel, B. Wolter, K. V. Bergmann, A. Kubetzka, and R. Wiesendanger, Science **341**, 636 (2013).

[12] F. Jonietz, S. Mühlbauer, C. Pfleiderer, A. Neubauer, W. Münzer, A. Bauer, T. Adams, R. Georgii, P. Böni, R. A. Duine, K. Everschor, M. Garst, and A. Rosch, Science **330**, 1648 (2010).

[13] Y. Ishikawa and M. Arai, J. Phys. Soc. Jpn. **53**, 2726 (1984).

[14] W. Münzer, A. Neubauer, T. Adams, S. Mühlbauer, C. Franz, F. Jonietz, R. Georgii, P. Böni, B. Pedersen, M. Schmidt, A. Rosch, and C. Pfleiderer, Phys. Rev. B **81**, 041203(R) (2010).

[15] X. Z. Yu, Y. Onose, N. Kanazawa, J. H. Park, J. H. Han, Y. Matsui, N. Nagaosa, and Y. Tokura, Nature (London) **465**, 901 (2010).

[16] X. Z. Yu, N. Kanazawa, Y. Onose, K. Kimoto, W. Z. Zhang, S. Ishiwata, Y. Matsui, and Y. Tokura, Nat. Mater. **10**, 106 (2011).

[17] H. Wilhelm, M. Baenitz, M. Schmidt, U. K. Rößler, A. A. Leonov, and A. N. Bogdanov, Phys. Rev. Lett. **107**, 127203 (2011).

[18] B. Lebech, J. Bernhard, and T. Freltoft, J. Phys. Condens. Matter **1**, 6105 (1989).

[19] S. Seki, X. Z. Yu, S. Ishiwata, and Y. Tokura, Science **336**, 198 (2012).

[20] T. Adams, A. Chacon, M. Wagner, A. Bauer, G. Brandl, B. Pedersen, H. Berger, P. Lemmens, and C. Pfleiderer, Phys. Rev. Lett. **108**, 237204 (2012).

[21] Y. Tokunaga, X. Z. Yu, J. S. White, H. M. Rønnow, D. Morikawa, Y. Taguchi, and Y. Tokura, Nat. Commun. **6**, 7638 (2015).

[22] A. S. Sukhanov, A. Heinemann, L. Kautzsch, J. D. Bocarsly, S. D. Wilson, C. Felser, and D. S. Inosov, Phys. Rev. B **102**, 140409(R) (2020).

[23] Y. Togawa, T. Koyama, K. Takayanagi, S. Mori, Y. Kousaka, J. Akimitsu, S. Nishihara, K. Inoue, A. S. Ovchinnikov, and J. Kishine, Phys. Rev. Lett. **108**, 107202 (2012).

[24] S. Mankovsky, S. Polesya, H. Ebert, and W. Bensch, Phys. Rev. B **94**, 184430 (2016).

[25] K. T. Ko, K. Kim, S. B. Kim, H. D. Kim, J. Y. Kim, B. I. Min, J. H. Park, F. H. Chang, H. J. Lin, A. Tanaka, and S. W. Cheong, Phys. Rev. Lett. **107**, 247201 (2011).

[26] N. J. Ghimire, M. A. McGuire, D. S. Parker, B. Sipos, S. Tang, J. Q. Yan, B. C. Sales, and D. Mandrus, Phys. Rev. B **87**, 104403 (2013).

[27] A. C. Bornstein, B. J. Chapman, N. J. Ghimire, D. G. Mandrus, D. S. Parker, and M. Lee, Phys. Rev. B **91**, 184401 (2015).

[28] N. Sirica, S. K. Mo, F. Bondino, I. Pis, S. Nappini, P. Vilmercati, J. Yi, Z. Gai, P. C. Snijders, P. K. Das, I. Vobornik, N. Ghimire,

M. R. Koehler, L. Li, D. Sapkota, D. S. Parker, D. G. Mandrus, and N. Mannella, Phys. Rev. B **94**, 075141 (2016).

[29] N. Sirica, P. Vilmercati, F. Bondino, I. Pis, S. Nappini, S. K. Mo, A. V. Fedorov, P. K. Das, I. Vobornik, J. Fujii, L. Li, D. Sapkota, D. S. Parker, D. G. Mandrus, and N. Mannella, Commun. Phys. **3**, 65 (2020).

[30] P. Giannozzi *et al.*, J. Phys. Condens. Matter **21**, 395502 (2009).

[31] G. Kresse and J. Furthmüller, Phys. Rev. B **54**, 11169 (1996).

[32] J. P. Perdew, K. Burke, and M. Ernzerhof, Phys. Rev. Lett. **77**, 3865 (1996).

[33] D. W. Shen, Y. Zhang, L. X. Yang, J. Wei, H. W. Ou, J. K. Dong, B. P. Xie, C. He, J. F. Zhao, B. Zhou, M. Arita, K. Shimada, H. Namatame, M. Taniguchi, J. Shi, and D. L. Feng, Phys. Rev. Lett. **101**, 226406 (2008).

[34] See Supplemental Materials at http://link.aps.org/supplemental/10.1103/PhysRevB.106.035129 for (i) details about the fit of energy distribution curves (EDCs) and MDCs, (ii) comparison between the experimental and calculated band structures near the Fermi level, and (iii) the calculated band structure of $Cr_{1/3}NbS_2$ with different Coulomb interaction between Cr atoms, which includes Refs. [45–47].

[35] D. E. Eastman, F. J. Himpsel, and J. A. Knapp, Phys. Rev. Lett. **40**, 1514 (1978).

[36] E. Kisker, K. Schröder, M. Campagna, and W. Gudat, Phys. Rev. Lett. **52**, 2285 (1984).

[37] P. Aebi, T. J. Kreutz, J. Osterwalder, R. Fasel, P. Schwaller, and L. Schlapbach, Phys. Rev. Lett. **76**, 1150 (1996).

[38] D. E. Shai, C. Adamo, D. W. Shen, C. M. Brooks, J. W. Harter, E. J. Monkman, B. Burganov, D. G. Schlom, and K. M. Shen, Phys. Rev. Lett. **110**, 087004 (2013).

[39] X. Xu, Y. W. Li, S. R. Duan, S. L. Zhang, Y. J. Chen, L. Kang, A. J. Liang, C. Chen, W. Xia, Y. Xu, P. Malinowski, X. D. Xu, J. H. Chu, G. Li, Y. F. Guo, Z. K. Liu, L. X. Yang, and Y. L. Chen, Phys. Rev. B **101**, 201104(R) (2020).

[40] W. Eberhardt, E. W. Plummer, K. Horn, and J. Erskine, Phys. Rev. Lett. **45**, 273 (1980).

[41] T. J. Kreutz, T. Greber, P. Aebi, and J. Osterwalder, Phys. Rev. B **58**, 1300 (1998).

[42] E. M. Clements, R. Das, L. Li, P. J. Lampen-Kelley, M.-H. Phan, V. Keppens, D. Mandrus, and H. Srikanth, Sci. Rep. **7**, 6545 (2017).

[43] H. Han, L. Zhang, D. Sapkota, N. Hao, L. Ling, H. Du, L. Pi, C. Zhang, D. G. Mandrus, and Y. Zhang, Phys. Rev. B **96**, 094439 (2017).

[44] I. N. Bhatti, I. N. Bhatti, R. N. Mahato, and M. A. H. Ahsan, Phys. Lett. A **383**, 2326 (2019).

[45] S. Shi, A. L. Wysocki, and K. D. Belashchenko, Phys. Rev. B **79**, 104404 (2009).

[46] E. Şaşıoğlu, C. Friedrich, and S. Blügel, Phys. Rev. B **83**, 121101(R) (2011).

[47] L. Vaugier, H. Jiang, and S. Biermann, Phys. Rev. B **86**, 165105 (2012).